

Supplement of Atmos. Meas. Tech., 8, 4539–4559, 2015
<http://www.atmos-meas-tech.net/8/4539/2015/>
doi:10.5194/amt-8-4539-2015-supplement
© Author(s) 2015. CC Attribution 3.0 License.



Supplement of

Local- and regional-scale measurements of CH₄, δ¹³CH₄, and C₂H₆ in the Uintah Basin using a mobile stable isotope analyzer

C. W. Rella et al.

Correspondence to: C. W. Rella (rella@picarro.com)

The copyright of individual parts of the supplement might differ from the CC-BY 3.0 licence.

S1 Deviations from an Ideal Spectrometer

CRDS, being a time-based measurement and a direct measurement of absorbance, is a highly linear and stable technology. However, even these spectrometers can have small imperfections that can affect the measurements. We discuss the following possible spectrometer errors: absorption loss offsets ε_{12} and ε_{13} , and nonlinearity in the absorbance scale.

S1.1 Absorption loss offsets

In the CRDS instruments described here, the measurement of the peak height of the absorption line is used as a quantitative measure of the mole fraction of the target species. The peak height is determined from the measured spectrogram by a nonlinear fit to model spectral functions, and it is defined as the difference between the loss at the peak of the absorption line and the loss at this same wavelength *without the analyte gas present* (called the baseline absorption). It is highly impractical to remove the analyte gas entirely from the optical cavity during operation; instead, the baseline absorption is determined from the nonlinear fit itself. Note that this baseline is not zero – it is a finite value that includes the transmission, absorption, and scattering losses of the optical mirrors¹. If the baseline loss is not reproduced well by the spectral fit to the spectrogram (this can occur if the empty cavity response of the instrument is not spectrally flat; i.e., the baseline loss depends on laser wavelength), then there can be a non-zero absorption loss offset, α_{offset} :

$$\alpha_{true} = \alpha_{measured} + \alpha_{offset} \quad (S1)$$

Note that for the individual species $^{12}\text{CH}_4$ and $^{13}\text{CH}_4$, this term leads directly to Eqs. (S1) and (Main Text 7), where $k_{12}\alpha_{^{12}\text{C} offset} = \varepsilon_{12}$ and $k_{13}\alpha_{^{13}\text{C} offset} = \varepsilon_{13}$; this absorption offset is the physical origin of the concentration offsets ε_{12} and ε_{13} . We begin with Main Text Eq. 5, reproduced here:

$$\delta^{13}\text{CH}_4 = 1000 \left(\frac{k_{13}\alpha_{13} + \varepsilon_{13}}{(k_{12}\alpha_{12} + \varepsilon_{12}) r_{VPDB}} - 1 \right) \quad (S2)$$

Given that $\varepsilon_{12} \ll k_{12}\alpha_{12}$ (due to the fact that the $^{12}\text{CH}_4$ line is so large), and using the approximation $\frac{1}{1+x} \sim 1 - x + \mathcal{O}(x^2)$... for small x , we can rewrite the equation, keeping terms to first order in ε_i :

$$\delta^{13}\text{CH}_4 = \frac{1000}{r_{VPDB}} \left[\frac{\frac{k_{13}}{k_{12}}\alpha_{13} + \left(\varepsilon_{13}\frac{1}{k_{12}} - \varepsilon_{12}\frac{k_{13}\alpha_{13}}{k_{12}^2\alpha_{12}} \right) + \dots}{\alpha_{12}} \right] - 1000 \quad (S3)$$

¹ The baseline also includes the absorption, resonant or non-resonant, from other gases in the cavity. We will consider these effects below, in the section on cross-interference.

We define a net absorption loss offset parameter $\alpha_0 \equiv \varepsilon_{13} \frac{1}{\kappa_{12}} - \varepsilon_{12} \frac{\kappa_{13} \alpha_{13}}{\kappa_{12}^2 \alpha_{12}}$. Note that the first term does not depend on the gas concentration or the isotope ratio of the sample, and the second term depends on the isotope ratio (but not the gas concentration). In addition, the second term is substantially smaller than the first, since $\frac{\kappa_{13} \alpha_{13}}{\kappa_{12}^2 \alpha_{12}}$ is the isotope ratio itself, or about 1.1% in most samples. We will therefore consider α_0 to be independent of concentration and isotope ratio to first order.

Equation (S3) simplifies to the following expression.

$$\delta^{13}\text{CH}_4 = \frac{1000}{r_{VPDB}} \left[\frac{k_{13} \alpha_{13}}{k_{12} \alpha_{12}} + \frac{\alpha_0}{\alpha_{12}} \right] - 1000 \quad (\text{S4})$$

Comparing this equation with Eq. (6) in the main text, we see an additional term. Note that this term is inversely proportional to the loss of the $^{12}\text{CH}_4$ line, and thus inversely proportional to methane concentration.

S1.2 Absorption loss nonlinearity

CRDS has been shown to provide highly linear measurements of gas mole fractions (Richardson et al. 2012), but at very high loss, the ringdown time is short ($< 5 \mu\text{sec}$), and we expect that nonlinearities due to e.g., the non-zero shut-off time of the laser and the response time of the ringdown detector, may become evident. We model the nonlinearity as a (weak) nonlinear dependence of the observed $^{13}\text{CH}_4$ absorbance on the $^{12}\text{CH}_4$ absorbance, or $\alpha_{13} \Rightarrow \alpha_{13} + \beta \alpha_{12} + \gamma \alpha_{12}^2$, which, when substituted in Eq. (S4), leads to

$$\{\delta^{13}\text{CH}_4\}_{\text{spectr. corr}} = \frac{1000}{r_{VPDB}} \left[\frac{k_{13} \alpha_{13}}{k_{12} \alpha_{12}} + \gamma \frac{k_{13} \alpha_{12}}{k_{12}} + \frac{\alpha_0}{\alpha_{12}} \right] + \left(\frac{1000}{r_{VPDB}} \frac{k_{13}}{k_{12}} \beta - 1000 \right) \quad (\text{S5})$$

Eq. (S5) shows the effect of the nonlinearity on the determination of $\delta^{13}\text{CH}_4$. If we assume that the calibration coefficients are constants (i.e., $k_{12} = \kappa_{12}$ and $k_{13} = \kappa_{13}$), and if we grouping terms and substitute for the calibration terms \mathbf{A}' and \mathbf{B}' , we find:

$$\{\delta^{13}\text{CH}_4\}_{\text{spectr. corr}} = \mathbf{A}' \frac{\alpha_{13}}{\alpha_{12}} + \frac{\mathbf{A}' \gamma}{\kappa_{12}} c_{12} + \frac{1000 \kappa_{12} \alpha_0}{r_{VPDB}} \frac{1}{c_{12}} + \left(\frac{1000}{r_{VPDB}} \frac{\kappa_{13}}{\kappa_{12}} \beta - 1000 \right), \text{ leading to}$$

$$\{\delta^{13}\text{CH}_4\}_{\text{spectr. corr}} = \mathbf{A}' \frac{\alpha_{13}}{\alpha_{12}} + \mathbf{\Gamma} c_{12} + \frac{\mathbf{c}_0}{c_{12}} + \mathbf{B}'$$

$$\text{Where } \mathbf{A}' = \frac{1000 \left(\frac{\kappa_{13}}{\kappa_{12}} \right)}{r_{VPDB}}$$

$$\mathbf{B}' = \left(\frac{1000}{r_{VPDB}} \frac{\kappa_{13}}{\kappa_{12}} \beta - 1000 \right) = \mathbf{A}' \beta - 1000, \quad (\text{S6})$$

$$\mathbf{\Gamma} = \frac{\mathbf{A}' \gamma}{\kappa_{12}}, \text{ and}$$

$$\mathbf{c}_0 = \frac{1000 \kappa_{12} \alpha_0}{r_{VPDB}}$$

We first consider the term β . It incorporates not only the first order correction to the absorbance, but also any spectroscopic crosstalk from $^{12}\text{CH}_4$ onto the $^{13}\text{CH}_4$ measurement. Solving for β given \mathbf{A}' and \mathbf{B}' gives $\beta = 1.09 \times 10^{-4}$. Another way of looking at this term is to realize that for an ideal spectrometer, the term \mathbf{B}' should equal -1000.0 ‰. It is in fact about about 1.7% more positive. Although it is possible that this is due to a nonlinearity of the absorption scale, it is more likely to be due to the process by which the complicated $^{12}\text{CH}_4$ model function that underlies the $^{13}\text{CH}_4$ line was generated. As we noted, if we made an error in the removal of the $^{13}\text{CH}_4$ lines, then that would mean that the measurement of the peak loss for $^{13}\text{CH}_4$ would include contributions from the concentration of both isotopologues.

We now turn our attention to the other two terms, Γ and c_0 . Both of these terms induce a dependence of $\delta^{13}\text{CH}_4$ on methane concentration. We have performed an experiment to investigate the concentration dependence, using the setup shown in Fig. S1. Two off-the-shelf mass flow controllers (Sierra SmartTrak 50 Series, Sierra Instruments, Monterey, CA) were used to generate different mixtures of variable methane content. The total flow was greater than the flow drawn by the instrument, with the remainder of the gas directed to an open split so that the instrument inlet pressure was approximately ambient pressure. Each concentration step was five minutes, and the methane was varied from about 2 – 20 ppm and back 12 steps over about an hour. This cycle was repeated fifteen times.

The time series obtained, using the isotopic instrument FCDS2016, is shown in Fig. S2, on the left panels. A clear bias is visible in the 1-minute average of $(\delta^{13}\text{CH}_4)_{raw}$. These data are fit to the second expression in Eqs. (S5). We perform a fit in which c_0 and Γ are free parameters in the linear least squares fit (assuming that \mathbf{B}' is constant). We perform this fit a second time with Γ set to zero, to assess the degree to which nonlinearity is an effect. In both cases, the true $\delta^{13}\text{CH}_4$ of the cylinder is also an adjustable fit parameter. The results of these two fits are shown in the right panel of Fig. S2, and the parameters are summarized in Table S1.

Table S1: Summary of the concentration dependent isotope correction coefficients, expressed in terms of the optical loss, both with and without nonlinear correction. See text for discussion.

Parameter	including absorbance nonlinearity	without absorbance nonlinearity	Comments
c_0	-11.38 ± 0.34 [‰ – ppm]	-12.75 ± 0.20 [‰ – ppm]	Net concentration offset parameter. This parameter is instrument specific, and can vary over time
Γ	$+0.027 \pm 0.006$ [‰/ppm]	--	Second order absorbance nonlinearity
Tank Value	-38.91 ± 0.14 ‰	-39.34 ± 0.03 ‰	Cylinder value generated by fit process

First, we consider the net concentration offset. As can be seen from Fig. S2, the offset c_0 is the dominant source of error in $\delta^{13}\text{CH}_4$ with varying CH_4 concentration. At 2 ppm, this term shifts the reported isotope ratio by about 6 ‰. This term has a few important characteristics:

- 1) Because this term is due to spectrometer imperfections, this term is *instrument-specific*.
- 2) This term can in principle drift over time, and be influenced by external environmental parameters, such as ambient temperature or pressure, leading to drift in the instrument.

How big an effect is the nonlinearity? At 18 ppm CH₄, the highest methane concentration considered in this experiment, this term shifts the isotope ratio by about 0.50 %. In terms of optical absorbance, this value corresponds to a loss nonlinearity γ of 7.9×10^{-10} [ppb/cm]⁻¹. In real terms, that means that at the highest concentration of 18 ppm, where $\alpha_{12} \sim 4,000$ ppb / cm, the ratio $\frac{\alpha_{13}}{\alpha_{12}}$ is shifted by $\gamma\alpha_{12} = -3.1 \times 10^{-6}$. The apparent result of the nonlinearity is that the ratio is underestimated, which means that α_{12} is slightly overestimated; i.e., the reported ringdown time is slightly *shorter* than expected. The physical source(s) of this nonlinearity has not been identified. Typically, this small nonlinearity is ignored, but for very careful measurements over a wide range of concentrations, this nonlinear term can be included. Because it is driven by electronic and optical processes which are not necessarily controlled during the assembly of the spectrometer, this parameter should be measured on a per-instrument basis.

S2 Cross interference from other gas species

Cross-interference between different species in the gas mixture is caused by one of three fundamental categories: 1) direct absorption, 2) analyte spectral lineshape effects, or 3) background spectral lineshape effects.

Direct Absorption: According the Beer-Lambert Law, the absorbance at a given frequency is given by the simple sum of the individual absorbances from each of the absorption lines in the spectrum. Thus, to first order, variations in the background gas matrix should not affect the measurement of the primary analyte species. However, if the model does not correctly account for the absorbance spectrum of a background gas component, there will be an error in the fit which manifests as a bias on the analyte measurement that is proportional to the *background gas species*. In other words, direct absorption adds an offset term ε to Eq. (S1) that depends linearly on the mole fraction of the background gas species.

$$c = k\alpha + \varepsilon_{bkg \text{ species}} \quad (S7)$$

Analyte Spectral Lineshape Effects: There are three principal mechanisms that determine the spectral line shape for isolated ro-vibrational lines, such as those used in the CRDS instrumentation discussed here: Doppler broadening, Lorentzian broadening, and Dicke line narrowing (Varghese and Hanson 1984). The Doppler broadening coefficient is an intrinsic property of the analyte molecule (i.e., its mass and temperature), and does not depend on the constituents of the background gas composition. However, the Lorentzian broadening and Dicke line narrowing effects do depend both on the analyte gas and on the constituents of the background gas composition. Thus, for example, if the oxygen in the background matrix is replaced with nitrogen, even though neither gas absorbs in this spectral region, the spectrum of the methane will change. In a spectroscopic measurement, the total area of the spectral line is conserved throughout this process. However, this CRDS analyzer uses peak height rather than area as a quantitative measure of the ¹²CH₄ and ¹³CH₄ concentrations, due to the fact that the

measurement of peak height is more precise and more stable than the area measurement. As a result, the peak height of the absorption features can have a systematic bias as the background gas mixture varies, due to both the line broadening and line narrowing effects.

The magnitude of the cross-interference due to spectral broadening depends both on the concentration of the background species (perhaps nonlinearly, because the broadening effect is not always a linear process) *and* the analyte species (typically linearly, because the error introduced by a lineshape error is proportional to the concentration of the analyte species). Thus, in Eq. (S1), the term k depends on the concentration of the background species (perhaps in a nonlinear fashion). In practice, the magnitude of the effect is significant only for gases that comprise a significant fraction (>0.1%) of the total, which in most situations is restricted to N₂, O₂, Ar, and H₂O (and, in some cases, carbon dioxide). It is important to remember that the analyte gas itself can also represent a large fraction of the background gas, which can also affect its lineshape. This effect is called self-broadening.

Background spectral lineshape effects: The same processes that cause distortions in the lineshape of the analyte gas can also affect the lineshapes of nearby absorption lines of other background gas species. If these lineshape effects, if not properly accounted for in the spectral model used in the fitting process, can lead to unexpected residuals in the fit, and in turn lead to biases in the reported analyte peak height. The effect of broadening on the analyte gas measurement are a) proportional to the concentration of gas corresponding to the nearby absorption line, and b) proportional to the concentration of the background gas that is changing the broadening, but c) independent of the analyte gas concentration. In other words, background spectral lineshape effects modifies the term ϵ .

Using these general categories, we now discuss how ¹²CH₄, ¹³CH₄, and δ^{13} CH₄ are determined from the spectroscopic measurements.

S2.1 ¹²CH₄

Direct Absorption: The only clear source of direct absorption in the ¹²CH₄ region is H₂O, which clearly has measureable absorption in the vicinity of the ¹²CH₄ feature but is not included in the model function. This cross-interference was investigated in Rella et al. 2013, and was determined to be +1.017 ppb CH₄/ % H₂O. We estimate the uncertainty of this measurement to be about 0.5 ppb CH₄. No measurements have been made of the cross-talk of CO₂ onto ¹²CH₄, but the HITRAN database (which is well benchmarked for CO₂) shows no nearby lines that should affect the ¹²CH₄ measurement significantly. On this basis, we estimate the direct cross-interference from CO₂ to be << 1 ppb ¹²CH₄ / 1000 ppm CO₂.

Analyte Spectral Lineshape Effects: The inert gases N₂, O₂, Ar have been investigated in Nara et al. 2012, and under most ambient conditions, their effect can be ignored, although their effect can be measureable if synthetic air standards are used. The effect of these gases is expressed as follows (following Nara et al. 2012):

$$c_{12act} = c_{12measured} \cdot (1 + a_{O_2 \rightarrow c_{12}} \cdot c_{O_2} + a_{Ar \rightarrow c_{12}} \cdot c_{Ar}) \quad (S8)$$

In Nara et al. 2012, data are reported for three models of CRDS analyzer. For the most recent model, the values for the coefficients are $a_{O_2 \rightarrow c_{12}} = 2.36 \times 10^{-4} / \% O_2$ and $a_{Ar \rightarrow c_{12}} = 5.67 \times 10^{-4} / \% Ar$.

Water vapor is a more significant source of lineshape errors. H₂O exists in the atmosphere at mole fractions of 0 – 4% or higher, which can lead to significant cross-interference due to spectral broadening. In addition, because water is a volatile species that can variably dilute the long-lived species, atmospheric scientists typically report the so-called dry-mole fraction of ¹²CH₄, or the mole fraction that would exist if all the water were removed. The cross-interference effect of H₂O due to broadening and dilution on ¹²CH₄ has been investigated in detail in Chen et al. 2010, Nara et al. 2012, and Rella et al. 2013. The dry mole fraction of ¹²CH₄ is determined from the so-called ‘wet’ value using the following expression:

$$\frac{c_{12_{wet}}}{1+dH_{rep}+eH_{rep}^2} = c_{12_{dry}} \quad (S9)$$

The ¹²CH₄ measurements in this work are derived from the same spectra as in the above references. However, the water vapor measurements are not the same between the two instrument designs, and the cavity pressure is slightly different, resulting in slightly different coefficients. Experiments were performed using methodologies described in Rella et al. (2013) and the coefficients were determined to be $d = -0.01188$ and $e = 3.17 \times 10^{-4}$. As expected, these are similar to the Chen et al. (2010) coefficients of -9.823×10^{-3} and 2.39×10^{-4} .

Background Spectral Lineshape Effects: There are no strong background gas absorption features in the vicinity of the ¹²CH₄ line, so these background gas effects are not expected to play a role here.

Thus, we may summarize the determination of ¹²CH₄ as follows:

$$c_{12_{dry}} = \frac{\kappa_{12}(1+a_{O_2 \rightarrow c_{12}} \cdot c_{O_2} + a_{Ar \rightarrow c_{12}} \cdot c_{Ar})\alpha_{12}}{1+dH_{rep}+eH_{rep}^2} + \varepsilon_{H_{rep} \rightarrow c_{12}} \cdot H_{rep} \quad (S10)$$

Where $\kappa_{12} = 4.333$ ppb ¹²CH₄ / (ppb/cm)

$d = -0.01188$ / % H_{rep}

$e = 3.17 \times 10^{-4}$ / (% H_{rep})²

$a_{O_2 \rightarrow c_{12}} = +2.58 \pm 0.17 \times 10^{-4}$ / % O₂ / ppb ¹²CH₄ (Nara et al. 2012) (S11)

$a_{Ar \rightarrow c_{12}} = +5.93 \pm 0.36 \times 10^{-4}$ / % Ar / ppb ¹²CH₄ (Nara et al. 2012)

$\varepsilon_{H_{rep} \rightarrow c_{12}} = +1.02 \pm 0.5$ ppb ¹² CH₄ / % H₂O (Rella et al. 2013)

Only the contribution of the κ_{12} , d , and e terms are included in the instrument software. The influence of other terms must be computed by the user in a post-processing step.

S2.2 ¹³CH₄

S2.2.1 The effect of background gases

Now we consider the effects of the gas matrix. Returning to Eq. (S5), we see that the coefficient of first term in the numerator ($\frac{\kappa_{13}}{\kappa_{12}}$) represents analyte spectral lineshape effects. To the extent that the effects of broadening are the same on both methane species, then this ratio reduces to the constant $\frac{\kappa_{13}}{\kappa_{12}}$. However, if the broadening does not influence both species identically, the ratio may then vary with the background gas mixture. We perform a first order Taylor series expansion on the ratio for all background species:

$$\frac{\kappa_{13}}{\kappa_{12}} \sim \frac{\kappa_{13}}{\kappa_{12}} + \sum_{i=all} \frac{\partial(\kappa_{13}/\kappa_{12})}{\partial(c_i)} c_i \quad (S12)$$

The partial derivatives represent the effect of the different gas components on the ratio of the peak heights of the two CH₄ species. We recast this equation as follows to more clearly indicate the fractional change in the peak height ratios:

$$\frac{\kappa_{13}}{\kappa_{12}} \sim \frac{\kappa_{13}}{\kappa_{12}} [1 + \sum_{i=all} a_i c_i] \quad (S13)$$

The second term in the numerator of Eq. (S5) has influence of both direct absorption and background species lineshape effects (via ε_i) as well as from analyte species lineshape effects (via k_i). This term is fairly complex, but we may again perform a first order Taylor series expansion for all background species:

$$\varepsilon_{13} \frac{1}{\kappa_{12}} - \varepsilon_{12} \frac{\kappa_{13} \alpha_{13}}{\kappa_{12}^2 \alpha_{12}} \equiv f = f_0 + \sum_{i=all} \left(\frac{\partial f}{\partial c_i} \right) c_i = \alpha_0 + \sum_{i=all} b_i c_i \quad (S14)$$

The constant α_0 , the net offset parameter, is zero in an ideal spectrometer, but is nonzero if the analyte model functions do not perfectly represent the spectrograms produced by the spectrometer. We will assume it to be zero to simplify the equations, but this term (corresponding to $c_0(t)$ in the treatment in the main paper) must be considered in any well-designed experiment.

We rewrite Eq. (S5) with Eqs. (S13) and (S14), to show that all the background gas corrections for $\delta^{13}\text{CH}_4$ are applied to the $^{13}\text{CH}_4$ peak absorbance α_{13} , either as a multiplicative or an additive factor. Higher order terms and cross-terms can be added to the numerator if deemed necessary.

$$\{\delta^{13}\text{CH}_4\}_{all\ species} = A' \left[\frac{[1 + \sum_{i=all} a_i c_i] \alpha_{13} + \sum_{i=all} b_i c_i + \dots}{\alpha_{12}} \right] + B' \quad (S15)$$

The coefficients in Eq. (S15) a_i and b_i , are determined empirically from a series experiments where $\delta^{13}\text{CH}_4$ is held constant while the background gas species is varied. Calculating the partial derivative of the above equations provides a convenient way for relating observations to variations in the background gas mixture, and vice versa:

$$\frac{\partial}{\partial c_i} \delta^{13}\text{CH}_4 = A [a_i \alpha_{13} / \alpha_{12} + b_i / \alpha_{12}] \quad (S16)$$

The right side of Eq. (S16) should be evaluated under the conditions (i.e. $\delta^{13}\text{CH}_4 \sim \delta_0$) where the measurements are made. Noting that $A \frac{\alpha_{13}}{\alpha_{12}} = \delta_0 - \mathbf{B}'$ and that $\alpha_{12} \approx c_{12}/\kappa_{12}$, this simplifies to:

$$\frac{\partial}{\partial c_i} \delta^{13}\text{CH}_4 = (\delta_0 - \mathbf{B}')a_i + C_i/c_{12} \quad (\text{S17})$$

Where $C_i = \mathbf{A}'\kappa_{12}b_i$. Eq. (S17) is helpful because it predicts how $\delta^{13}\text{CH}_4$ is affected by different types of interference. Analyte lineshape changes appear as a shift in $\delta^{13}\text{CH}_4$ that is proportional to $(\delta_0 - \mathbf{B})$ (i.e., highly enriched samples will show a bigger effect). Interestingly, direct absorption (as well as indirect lineshape effects) exhibit a dependence that is inversely proportional to the $^{12}\text{CH}_4$ concentration. The tendency that interference tends to be larger at lower concentrations has important implications for detecting and correcting for these interferences.

Below, we describe several experiments designed to investigate dependence of the measurements of $\delta^{13}\text{CH}_4$ on background gas variations.

S2.2.2 Oxygen

Oxygen does not have any significant absorption features in this frequency range, so it only affects the lineshape of the analyte molecules. We performed a mixing experiment to measure the effect of oxygen on measurement of the isotope ratio. The setup used is shown schematically in Fig. S3. A 100 ppm CH_4 bottle (in a balance of air) with an isotope ratio of about -40 ‰ is diluted to 10 ppm using either zero air (which does not change the oxygen content) or with ultra high purity N_2 (which does). The flows were controlled with mass flow controllers. A shift in $\delta^{13}\text{CH}_4$ of $+3.25 \pm 0.3$ ‰ is observed when air is used to dilute instead of N_2 , corresponding to a net change in the oxygen content of $+18.8 \pm 1.9$ % O_2 . Thus, the overall effect is $+0.173 \pm 0.023$ ‰ / % O_2 (at $\delta_0 = -40$ ‰). Using Eq. (S17), we find $a_{\text{O}_2} = +1.71 \times 10^{-4}$ / % O_2 .

We compare this to the result from Nara et al. 2012. In that paper, it was found that the $^{12}\text{CH}_4$ has a oxygen broadening coefficient $+2.58 \pm 0.17 \times 10^{-4}$ / % O_2 / ppb $^{12}\text{CH}_4$. If the $^{13}\text{CH}_4$ measurement is not affected by water, then this entire effect would appear as a *decrease* in the isotope signature of -0.258 ‰. The fact that the isotope signature *increases* with oxygen indicates that the effect of oxygen on $^{13}\text{CH}_4$ is larger than the effect on $^{12}\text{CH}_4$, by about 67%. Qualitatively, this result is expected, given the heavier mass and thus narrower Doppler width of the $^{13}\text{CH}_4$ line, which in turn magnifies the effect of the change in the Lorentzian broadening due to the oxygen change. Quantitatively, the results are difficult to compare, due to the fact that neither of the two species have simple single-line absorption spectral, and they are fit with two different spectral algorithms that treat line broadening in a fundamentally different fashion.

Because oxygen is not measured directly in this instrument, this correction can only be applied in a post-acquisition data processing step, and only if the oxygen content is known or can be inferred via other means.

S2.2.3 Water Vapor

The primary isotopologue of water vapor, $^1\text{H}_2^{16}\text{O}$, is measured in real-time in this instrument. It is therefore possible to use this measurement to correct for the influence of water vapor on the isotope measurement. As discussed above, we look for the effect of water vapor on the isotope ratio rather than on the individual isotopologues of methane, using Eq. (S17). Because we have a spectroscopic measure of $c_{\text{H}_2\text{O}}$, we express Eq. (S10) in terms of the measured water vapor absorbance $\alpha_{\text{H}_2\text{O}}$, or

$$\{\delta^{13}\text{CH}_4\}_{\text{H}_2\text{O}} = \{\delta^{13}\text{CH}_4\}_{\text{uncorr}} + (\delta_0 - \mathbf{B}')\alpha_{\text{H}_2\text{O}} + \frac{c_{\text{H}_2\text{O}}}{c_{12}} \quad (\text{S18})$$

We look for two terms, $\alpha_{\text{H}_2\text{O}}$ and $C_{\text{H}_2\text{O}}$, that capture the direct analyte broadening and direct absorption effects, respectively. Because these two terms lead to different dependences of $\delta^{13}\text{CH}_4$ on methane concentration, their influence can be quantified by varying the water vapor concentration at different methane concentrations. The setup in Fig. S4 was used to generate air mixtures with variable humidity and methane. The flows through the mass flow controllers were adjusted such that the total flow delivered to the instrument port was greater than the instrument flow, such that the excess flow was disposed in an open split. For each of three water vapor levels, six different methane levels were generated every 7.5 minutes, both increasing and decreasing. The total cycle for all measurements was 4.5 hours, and was repeated 3 times in succession. Because the cylinder of 100 ppm methane is the only source of CH_4 in the mixture, the resulting mixture should have a constant $\delta^{13}\text{CH}_4$.

The upper left Fig S5 shows a time series of the total CH_4 , H_2O , and the lower left panel shows the raw $\delta^{13}\text{CH}_4$ signal prior to correction (i.e., using Eq. 12 from the main paper) for this experiment, as measured on one isotope analyzer (G2132-I, S/N: FCDS2016, Picarro, Inc.). The data indicate a strong dependence on both the CH_4 and H_2O concentrations. The error is greatest at low methane concentrations and high water vapor content. The blue points in the lower left panel are derived from the average of $(\delta^{13}\text{CH}_4)_{\text{raw}}$ over each ~ 7.5 minute segment, for each of the quasi-constant water vapor steps.

A least squares fit was performed to determine the coefficients. Included as a variable parameter in the fit is c_0 , the net concentration offset parameter. The residuals of the fit are shown in right panel of Fig S5, with the fit parameters $\alpha_{\text{H}_2\text{O}} = +8.72 \pm 0.39 \times 10^{-4} / \% \text{H}_2\text{O}$, $C_{\text{H}_2\text{O}} = +26.7 \pm 0.24 \text{‰} - \text{ppm} / \% \text{H}_2\text{O}$, and $c_0 = 12.54 \pm 0.36 \text{‰} - \text{ppm}$. The standard deviation of the residuals are 0.55 ‰.

The parameter $\alpha_{\text{H}_2\text{O}}$ represents the net effect of lineshape changes on the isotope ratio. The parameter is positive, which means that it is correcting for a negative effect of broadening on the ratio; i.e., with increasing water vapor concentration, delta tends to *lighter* or more negative values, indicating that the $^{13}\text{CH}_4$ line becomes broader relative to the $^{12}\text{CH}_4$ line with increasing water vapor. This result is expected, given the narrower Doppler width of the $^{13}\text{CH}_4$ line. At 1% water vapor, the net broadening effect is just 0.09‰ on the ratio (or 0.9 ‰). In Chen et al. (2010) and Rella et al. (2013), the broadening of the methane line $^{12}\text{CH}_4$ is shown to be only weakly affected by water vapor, compared to the CO_2 spectroscopic line that is used in those studies. The isotope ratio results indicate that the $^{13}\text{CH}_4$ is similarly weakly affected by water vapor.

The parameter C_{H_2O} represents the net effect of direct absorption on the isotope ratio. Note from Eq. (S14), this parameter depends primarily on the net direct absorbance effect of water on the two isotopologues to first order. At 1% water vapor, the net direct absorbance effect is 0.035 ppb / cm, or about 10 ‰ at 2 ppm CH₄ concentration. Note that the coefficient is positive indicating that it is compensating for a decrease in the reported isotope ratio as water vapor increases. Given that the magnitude of the effect is about 20 times greater than the effect observed on ¹²CH₄, most of the direct absorbance effect is due to model function errors in the ¹³CH₄ fit, and is due to the un-accounted for absorbance effect of nearby water lines.

Both parameters are included on the instrument; the parameters are determined using the test described here. Over the full range of water vapor and methane, we expect the correction to be good to about 1 ‰ or better. For experiments requiring the high accuracy, we recommend that the gas stream should be dried to <0.1 % water vapor content.

S2.2.4 Carbon Dioxide

There are weak ¹²C¹⁶O₂ lines in the vicinity of the ¹³CH₄ absorption feature. The relatively strong carbon dioxide line at 6056.6 wavenumbers is used for two purposes: a) to set the strength of the CO₂ lines in the 6029 wavenumber region during the fit of the ¹³CH₄, and b) to measure and correct for any residual influence of carbon dioxide on $\delta^{13}\text{CH}_4$. The calibration constant for this line, $\kappa_{CO_2} = \frac{c_{CO_2}}{\alpha_{CO_2}}$ was determined to be 7.78 ± 0.08 ppm CO₂ / [ppb / cm] after calibrated against gravimetric mixtures with an analytical uncertainty of 1%.

Following the treatment of water vapor, we look for a simple dependence of $(\delta^{13}\text{CH}_4)_{raw}$ on the carbon dioxide peak height α_{CO_2} , or

$$\{\delta^{13}\text{CH}_4\}_{CO_2} = \{\delta^{13}\text{CH}_4\}_{uncorr} + \frac{c_{CO_2}CO_2}{c_{12}} \quad (\text{S19})$$

In this expression, we consider only a direct absorbance effect. The setup we use is shown in Fig. S6. As in the water vapor experiment, for each of three CO₂ levels, six different methane levels were generated every 7.5 minutes, both increasing and decreasing in time. The total cycle time for all measurements was 4.5 hours. Because the cylinder of 100 ppm methane is the only source of CH₄ in the mixture, the resulting mixture should have a constant $\delta^{13}\text{CH}_4$. The data collected on this apparatus are shown Fig. S7, along with the fit to Eq. (S19), and the resulting fit parameters are $C_{CO_2} = -5.1 \pm 0.4 \times 10^{-3}$ ‰ – ppm CH₄ / ppm CO₂ and $c_o = 13.84 \pm 0.5$ ‰ – ppm CH₄. The residuals of the fit are 0.36 ‰, which includes the precision of each data point.

The parameter C_{CO_2} represents the net effect of direct absorption on the isotope ratio. For a 500 ppm change in the CO₂ concentration, the net direct absorbance effect is 1.25 ‰ at 2 ppm CH₄ concentration. Note that, the coefficient is positive which corrects the influence of CO₂ to decrease the reported isotope ratio. An additional fit that included a non-zero analyte broadening term a_{CO_2} was attempted, but the coefficient was zero within the uncertainty of the fit. This result is expected, given that CO₂

represents at most only about 0.2 % of the total background gas in these experiments. The parameter C_{CO_2} is determined for every instrument using this test, and included as a correction on the instrument.

S2.2.5 Ethane

It is clear from Fig. 1 in the main paper that there is potential for cross-interference on the $^{13}CH_4$ peak measurement from ethane. Given the fact that ethane is a common constituent in many fossil-fuel derived methane sources, such as natural gas or the emissions from O&G production or refining activities, it is important to characterize this interference.

Using the experimental spectrum shown in Fig. 1, a simple empirical spline model function was generated for use in the nonlinear fitting algorithms. The region from 6028.1 – 6029.1 wavenumbers is fit using this model function, along with model functions for methane, water vapor, and carbon dioxide. It is important to note that this fit in no way affects the fit of the $^{13}CH_4$, and the cross-interference of the ethane on $\delta^{13}CH_4$ is not incorporated into the software automatically.

The amplitude of the C_2H_6 model function was generated from a gravimetric mixture of 400 ppm ethane in synthetic air (Scott Specialty Gases, where), measured a different, functionally identical, instrument. The peak-to-valley loss difference is about 1.5 ppb / cm per ppm C_2H_6 . The uncertainty in the ethane calibration is 2% as quoted by the gas manufacturer.

In a one second measurement, the precision of the reported ethane concentration is 160 ppb, and the precision improves to about 45 ppb in a 1 minute average. How useful is this measurement? Consider a measurement of a sample of unprocessed or processed natural gas. Depending on the source, the ethane to methane ratio can vary from near 0% to more than 100%. For a sample containing 1 ppm of methane derived from natural gas, an ethane precision of 45 ppb in 1 minute corresponds to a measurement of the ethane-to-methane ratio with a precision of about 5%. Thus, it represents only a crude measurement of the ethane-to-methane ratio in most samples. However, even this relatively poor analytical precision be useful to correct the interference of ethane on to $\delta^{13}CH_4$, as we will discuss below.

There is of course the possibility of interference between the other gases and this measurement of ethane, which we investigate by injecting varying mixtures of CH_4 , CO_2 , and H_2O to determine the cross-interference of those gases on the ethane measurement, using similar configurations of cylinders and mass flow controllers as described above for $^{12}CH_4$ and $\delta^{13}CH_4$. We perform a simple linear correction of the reported ethane concentration which takes the form:

$$[C_2H_6]_{corrected} = [C_2H_6]_{raw} + a_{H_2O \rightarrow eth} H_2O + a_{CH_4 \rightarrow eth} CH_4 + a_{CO_2 \rightarrow eth} CO_2 \quad (S20)$$

The parameters that emerge from the analysis of the experimental data are $a_{H_2O \rightarrow eth} = 0.658$ ppm C_2H_6 / % H_2O , $a_{CH_4 \rightarrow eth} = +5.5 \pm 0.1 \times 10^{-3}$ ppm C_2H_6 / ppm CH_4 , and $a_{CO_2 \rightarrow eth} = +1.44 \pm 0.02 \times 10^{-4}$ ppm C_2H_6 / ppm CO_2 . There is a significant cross-interference due to water vapor. Cross interference with the other two gases is relatively small. We expect that the correction has an uncertainty of about 0.05 ppm C_2H_6 . Although we have considered the influence of the most common atmospheric constituents, there may

be interference from other gases in the atmosphere. These potential interferences have not been fully explored.

Finally, we investigate the interference of ethane onto the measurement of $\delta^{13}\text{CH}_4$. A bottle of 100 ppm ethane in air and a bottle of 100 ppm CH_4 in air were combined into a single flow in different ratios using two mass flow controllers. With only one source of methane in the experiment, the measurement of $\delta^{13}\text{CH}_4$ should be constant under all conditions. Instead, we see in Fig S8 that the reported $\delta^{13}\text{CH}_4$ is dependent on ethane, with a larger effect at smaller methane concentrations. We can therefore use an equation like Eq. (S19) to analyze these data, where we presume that at low levels (500 ppm C_2H_6), there is not a significant effect of broadening, and thus $a_{eth} = 0$:

$$\frac{\partial}{\partial c_{eth}} \delta^{13}\text{CH}_4 = C_{eth}/c_{12} \quad (\text{S21})$$

From analysis of the data in Fig. S8, we find that $C_{eth} = 35 \text{ ‰ ppm CH}_4 / \text{ppm C}_2\text{H}_6$. In other words, for an ethane-to-methane ratio of 10%, the effect on $\delta^{13}\text{CH}_4$ is + 3.5 ‰; i.e., the instrument tends to report heavier values for ethane-contaminated samples. Note that when isotopic analysis of a given sample is performed, where the assumption of a two-member mixing model can be applied, the effect of ethane is to offset the $\delta^{13}\text{CH}_4$ of the second member by a constant amount as specified by the expression above. This correction is not applied in the instrument software; it must be applied as a post-correction by the user during data analysis.

S2.2.6 Other Gas Species

Finally, we have considered the effect of a variety of different gases on the measurement of $\delta^{13}\text{CH}_4$, using a combination of experimental data and spectral databases such as HITRAN and the Pacific Northwest National Laboratory database (Johnson et al. 2004). The results are summarized in the Table below.

Note that we have only considered relatively small molecules, with fewer than about ten atoms in the molecule. Larger molecules have so many internal degrees of freedom that they do not have distinct ro-vibrational absorption lines. As a result, their infrared absorption spectra are broad and relatively featureless on the scale of the spectra that are used in the instrument, which means that their effect on the measurement of $\delta^{13}\text{CH}_4$ tends to be insignificant, at least at trace levels below about 500 ppm, whereupon broadening effects and background absorption effects can become important. A good example of such a molecule is propane. The effect of propane on $\delta^{13}\text{CH}_4$ is less than 0.1 ‰ / ppm C_3H_8 , with the uncertainty of the measurement limited by our ability to prepare and deliver a known sample to the instrument. Other large molecules, like longer-chain alkanes (butane, pentane, and so on) or aromatics (benzene, toluene, xylene, and so on), should have similarly small effects.

S3 Modeling the flow in the small volume AirCore during individual source sampling

A typical plume transect and reanalysis is shown in Fig. S9. In the left panel of the figure the initial transect of the plume is displayed. The FWHM of the plume is about two seconds, and there are only two points near the peak of the plume. The right panel shows the replay of the same pulse in red. Note that the pulse duration is much greater, that the peak height is much shorter, and the pulse has a trailing tail. We use a simple model to reconstruct the replayed pulse from the recorded data, consisting of the following three elements:

- 1) Time dilation equal to the ratio of the flows of recording and playback, or $1,500 \text{ sccm} / 60 \text{ sccm} = 25$.
- 2) A one sided exponential decay function (purple curve in the figure) to represent the gas response of the sampling system, with a time constant of 4.4 seconds.
- 3) A symmetric Gaussian broadening function (gray curve in the figure), with a Gaussian width of 1.0 seconds.

We simulate the replayed pulse by convolving the normalized exponential and Gaussian functions with the recorded pulse, and then stretch the time axis by a factor of 25. The resulting reconstructed pulse is shown as the black curve. Other than shifting the time axis to align the two curves, no adjustable parameters were used to fit the data.

The exponential decay dominates the time response of the system, decreasing the peak height by a factor of 2 and extending the pulse to long times. We expect that the 75cc mixing volume (which has a ~ 3 second flushing time at a flow 1,500 sccm) is the dominant source of finite gas response, but diffusion and velocity dispersion in the gas tube, the finite response time of the instrument may also contribute, and the chromatographic response of methane on the walls of the storage tube and sample delivery system will all play a role.

These dynamic processes may be different for each isotopologue; i.e., the heavier isotope may behave differently in this system, leading to fractionation in the isotopic response. For example, $^{13}\text{CH}_4$ has a different mass than $^{12}\text{CH}_4$, and therefore different gas diffusion coefficient. From Marrero and Mason (1972), we estimate that the diffusion coefficient for the heavier isotopologue to be about 2% smaller than the coefficient for $^{12}\text{CH}_4$ in air of $0.2 \text{ cm}^2 / \text{sec}$.

The top panel of Figure S10 displays a Keeling plot of $\delta^{13}\text{CH}_4$ vs CH_4^{-1} . There is a noticeable fractionation effect of a few permil that is most noticeable at the peak of the pulse, with the lighter isotopologue at the leading edge of the pulse the heavier isotopologue lagging the pulse. Without knowing the detailed mechanism behind the dispersion, it is difficult to generate a robust model of the dynamical behavior. However, we note empirically that if we simply delay the $^{13}\text{CH}_4$ pulse by about 0.5 seconds relative to the $^{12}\text{CH}_4$ pulse, the fractionation disappears; this is most clearly evident bottom panel of Fig. S10– the fractionation is no longer evident, and the R^2 has improved. We will use this time shift of 0.5 seconds for all the further analysis, although the difference between the two analysis methods is minimal; when the two analysis methods are applied to the sources measured, the difference in the results has a standard deviation of $\pm 0.8 \text{ ‰}$ and a bias of -0.37 ‰ , where including the time shift tends to report slightly lighter isotope ratios). One half a second in the replay is much smaller than the exponential time

constant of the replay ($4.4 \times 25 = 110$ seconds) or the Gaussian width ($1 \times 25 = 25$ seconds), and it is reasonable to expect this level of fractionation in this system.

The replayed ethane pulse is shown in Fig. S11, along with the methane pulse for reference on the same time axis. Although the ethane data are noisy, there is a distinct shift of the signal to later times of about 5 seconds. Ethane is a significantly heavier molecule with a lower diffusion coefficient, estimated to be 20% lower than that of methane using scaling laws in Marrero and Mason (1972). This difference is 10 times greater than the isotopic diffusion ratio of 2%, consistent with the fact that the observed 5 second shift is 10 times greater than the 0.5 second shift in the isotope ratio. We apply this 5 second shift for the following analysis, although we note that, because the precision requirement for the ethane / methane ratio is relaxed relative to $\delta^{13}\text{CH}_4$ (% vs ‰), this shift can be ignored. To quantify the ethane / methane ratio of the source, we perform a similar analysis of the measured ethane time series, with a linear regression between the observed ethane and methane concentrations. The C_2/C_1 ratio of 0.42 ± 0.2 is obtained from the linear regression of the data in the inset of Fig. S11.

The accuracy and repeatability of the plume sampling and reanalysis system was tested in the lab. Simulated plumes from a 100 ppm tank of methane were generated repeatedly. The following parameters were investigated: the width of the pulse (from 1 – 4 seconds), the location of the plume in the sampling tube at the instant when the flow is reduced for re-analysis, and the number of plumes captured in the tube simultaneously (1-3 plumes). $N = 25$ plumes were measured for each condition. Within the repeatability of the measurement (± 0.5 ‰), the results are statistically indistinguishable from each other, as well as from direct analysis of the bottle (after 10:1 dilution with zero air).

S4 Modeling the flow in the large volume AirCore during regional air sampling

We model the gas sampling system by the inlet pressure $P_I(t)$, the inlet flow $f_I(t)$, the storage volume V and pressure P_V , and the constant outlet flow f_O . The inlet flow is proportional to the pressure difference between the ambient and the storage vessel, or $f_I = K(P_I - P_V)$, where K is the conductance of the storage tube. The conductance of the tube can be calculated using Poiseuille's law for laminar flow in a circular tube (Bennett and Myers 1962):

$$K = \left[\frac{128\mu L}{\pi D^4} \right]^{-1} \quad (\text{S22})$$

where μ is the dynamic viscosity of air. For the storage tube alone, $K = 0.29$ sccm / Pa.

The pressure in the storage volume is related to the net flow into the volume by

$$\frac{dP_V}{dt} = \frac{1}{V} (f_I - f_O) P_V \quad (\text{S23})$$

We first consider a steady state condition with $P_I = P_{amb}$ and $\frac{dP_V}{dt} = 0$. In this case, $f_I = f_O$ and the pressure in the storage tube is a constant given by $P_C = P_{amb} - \frac{f_O}{K} = P_{amb} - P_{drop}$. For typical flows of 50 – 100 sccm, the pressure difference from ambient P_{drop} is typically about 200 Pa, or $2 \times 10^{-3} P_{amb}$.

For the low flows in this system and the small pressure changes expected at the inlet, we look for small deviations in the ambient and storage pressures, or $P_V = P_C + p_V(t)$ and $P_I = P_{amb} + p_I(t)$, where p_I and p_V are much smaller than P_{amb} .

Substituting for f_I , and keeping terms to first order in $p_V(t)$ and $p_I(t)$, we find the following expression:

$$\frac{dp_V}{dt} = \frac{KP_C}{V} (p_I - p_V) = r(p_I - p_V) \quad (S24)$$

The rate constant is given by $r = \frac{KP_{amb}}{V}$. Under typical conditions, r is about 0.01 sec⁻¹.

In the 1-D differential equation above, p_I is the forcing function of the system. Consider an ambient pressure change modeled by a Heaviside step function where $p_I = 0$ for $t < 0$ and $p_I = \rho_0$ for $t > 0$. The solution to this forcing function is

$$p_V(t) = \rho_0(1 - e^{-rt}) \quad (S25)$$

In other words, the pressure in the storage vessel rises from P_C at $t < 0$ to $P_C + \rho_0$ with a characteristic rate constant r . The inlet flow in this situation is given by

$$f_I = K(P_{drop} - \rho_0 e^{-rt}) = f_O - K\rho_0 e^{-rt} \quad (S26)$$

The flow returns to the steady state value with the same exponential recovery as the pressure. Since any forcing function $p_I(t)$ can be modeled by a sum of Heaviside functions (with different transition times and step sizes), we can then predict the inlet flow given arbitrary ambient conditions.

We will consider three sources of pressure variation in our model: altitude change, Bernoulli's effect, and a dynamic pressure effect akin to angle-of-attack lift on an aircraft wing:

$$p_I(t) = P_{amb}(1 - e^{-h/z_0}) - \frac{1}{2}R\rho v^2 \quad (S27)$$

In this equation, $h(t)$ is the altitude of the vehicle, z_0 is the scale height of the atmosphere (about 8,400 m), ρ is the mass density of air (1.2 kg / m³), v is the vehicle velocity, and the coefficient R captures the effect of the orientation of the inlet tube relative to the airflow around the vehicle. For a neutrally oriented tube, $R = 1$, and the simple form of Bernoulli's effect applies.

A separate experiment was performed to validate our ability to model the flow into the storage tube. In that experiment, a mass flow sensor (Model M-500SCCM-D, Alicat, Tucson, Arizona, USA) was located at the inlet to the storage tube during a drive, and the flow was measured along with the vehicle altitude and speed derived from GPS measurements. Figure S12 shows the results of this experiment. The

observed flows (purple curve in the central panel) were highly variable, due primarily to the rapid altitude changes encountered during the drive, with a mean of 64 sccm and a standard deviation of 26 sccm. We note that the highly variable flows observed caused by inlet pressure variations can be mitigated by installing a pressure controller at the inlet to the system to insulate the storage vessel from ambient pressure variability.

Using Eq. (S27) and the vehicle velocity derived from the GPS coordinates, we created a model for the inlet pressure $p_I(t)$, and by simulating this pressure as a series of Heaviside functions, we simulated the flow f_I (gray curve in the central panel). The four parameters that were adjusted to optimize the fit to the data are shown in Table S2.

Table S2: free parameters used to fit the measured flow data.

Parameter	Value	Notes
f_o	64.9 sccm	Outlet flow set by the needle valve at the outlet of the storage tube
K	0.065 sccm / Pa	System conductance, dominated by the flow meter inserted into the system.
R	0.35	Dynamic pressure coefficient, partially compensating for the negative pressure effect of Bernoulli's effect
Δt	23 seconds	Time shift between the two computers measuring the GPS coordinates and the flow meter

Note that K not only strongly affects the amplitude of the variations in the flow, it also affects the time constant, which can be seen most clearly when the vehicle stops in Fig S12. This relaxation provides an independent check of the validity of the model.

The value for K for the tubing (according to Eq. S22) is 0.29 sccm / Pa, and the value for the flow sensor (as specified by the manufacturer) is 0.076 sccm / Pa. The total K for the system is given by the reciprocal sum, or 0.060 sccm / Pa, which is reasonably close to the value 0.065 sccm / Pa as determined from the fit to the data. The value for $K = 0.065$ corresponds to a pressure drop of about 1000 Pa at the nominal flow of 65 sccm, and leads to a relaxation time $\frac{1}{r} = 153$ seconds for the system. Without the flow meter, the value of 0.29 sccm / Pa leads to a faster relaxation time of about 30 seconds.

For the regional isotope measurements performed in the Uintah Basin, a flow meter was not used. The flow through the system was set to about 85 sccm by adjusting the downstream needle valve in the vehicle. We model the flow using the GPS measurements of altitude and speed, using a value of K of 0.29. Typical results are presented in Fig S13 for data collected on 31 January, 2013, along with the altitude profile. With 95% of the flow variability due to altitude variations, ambient air will be somewhat over-sampled on the downhill segments of the drive relative to the uphill segments.

S5 Supplementary Materials: Figures

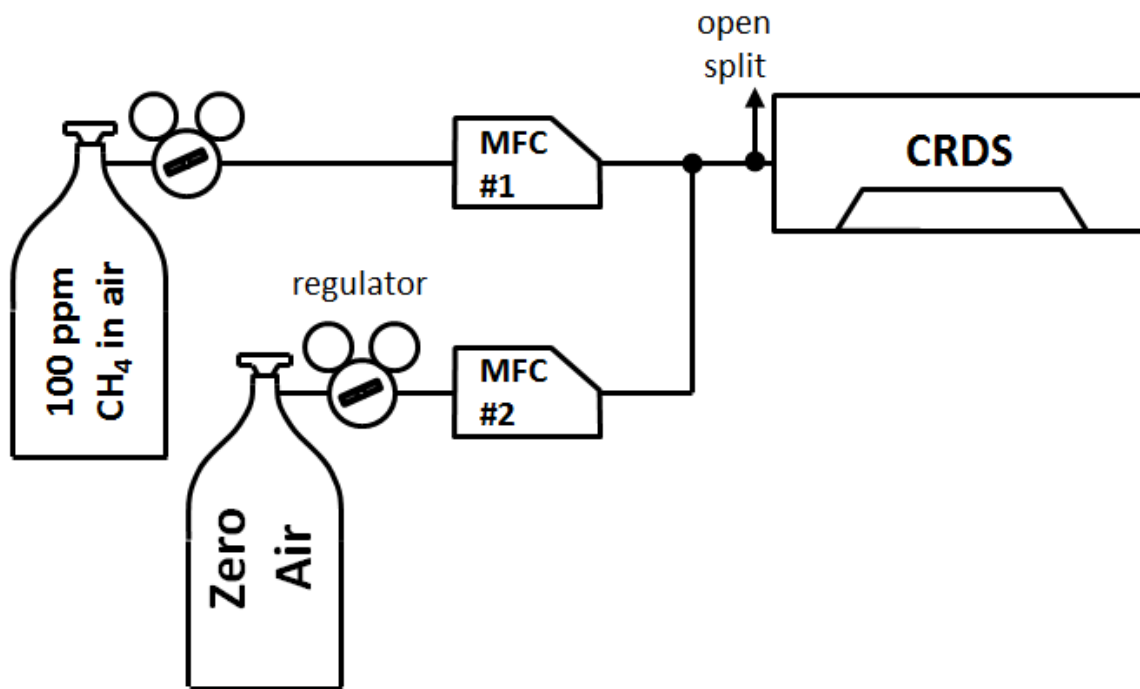


Fig S1: Setup for determining the concentration dependence of $\delta^{13}\text{CH}_4$. The flows through the two MFCs are adjusted to generate different mixtures of varying methane concentration

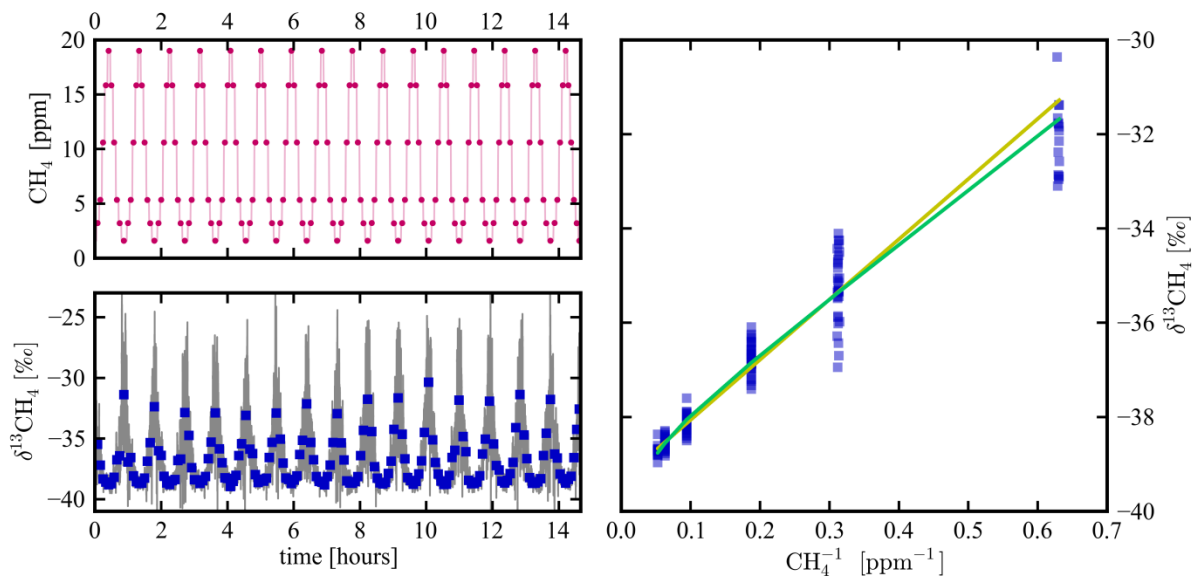


Fig S2: Data obtained on FCDS2016, using the apparatus in Fig 2. Top left: methane concentration series; bottom left: the 1-minute average of the raw $\delta^{13}\text{CH}_4$ signal, prior to correction (gray line), and average from each 7.5 minute segment (blue points). Right panel: $(\delta^{13}\text{CH}_4)_{\text{raw}}$ signal (blue points) as a function of the reciprocal of methane concentration. (brown curve) fit to data with a net concentration offset term of 12.77 ± 0.21 [‰ – ppm]. (green curve) fit to data with a net loss offset term of -11.41 ± 0.36 [‰ – ppm] and a nonlinearity of $+0.027 \pm 0.006$ [‰/ppm]. Generally, for concentrations below about 10 ppm, it is not necessary to include the nonlinearity, except for the most exacting application.

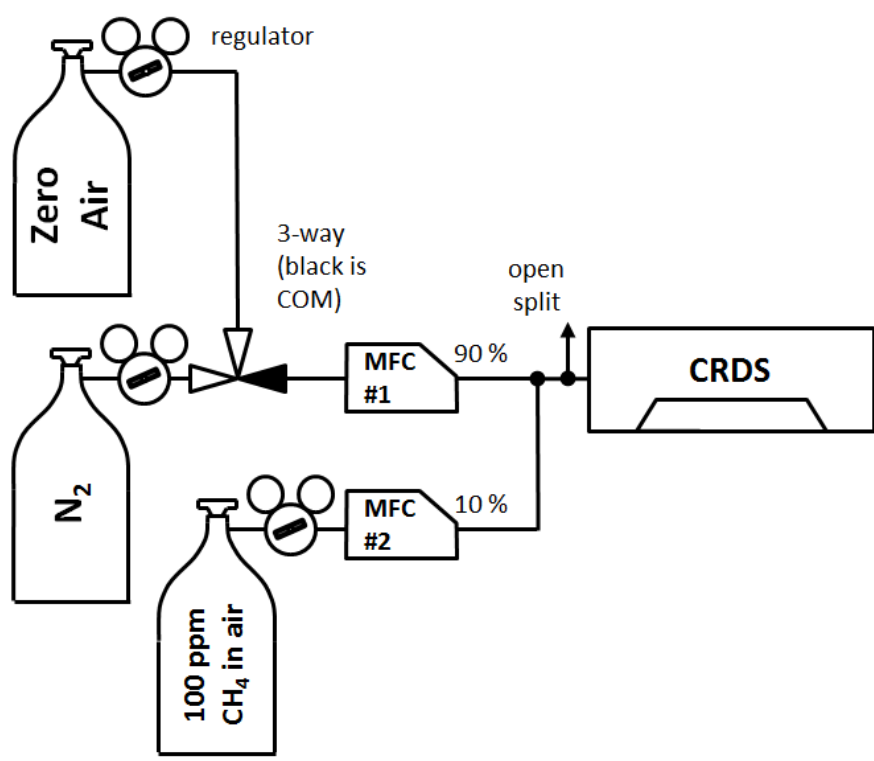


Figure S3: Apparatus for investigating the influence of oxygen on the isotopic measurement.

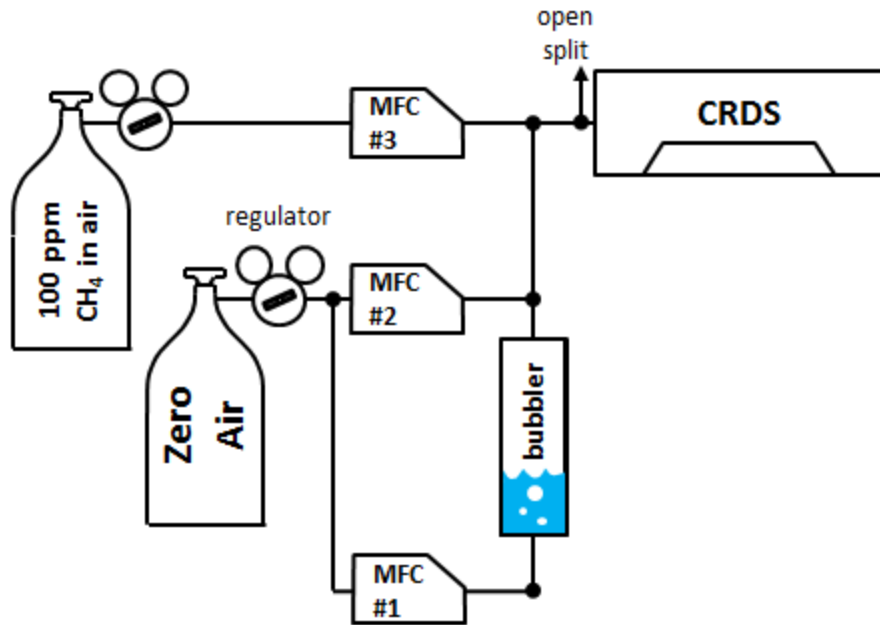


Figure S4: Setup for determining the water vapor cross-talk coefficients. The flows through the three MFCs are adjusted to generate different mixtures of dry and wet air, of varying methane concentration. The water vapor range covered with this system is 0 – 2.5%, and the methane range is 0 – 20 ppm.

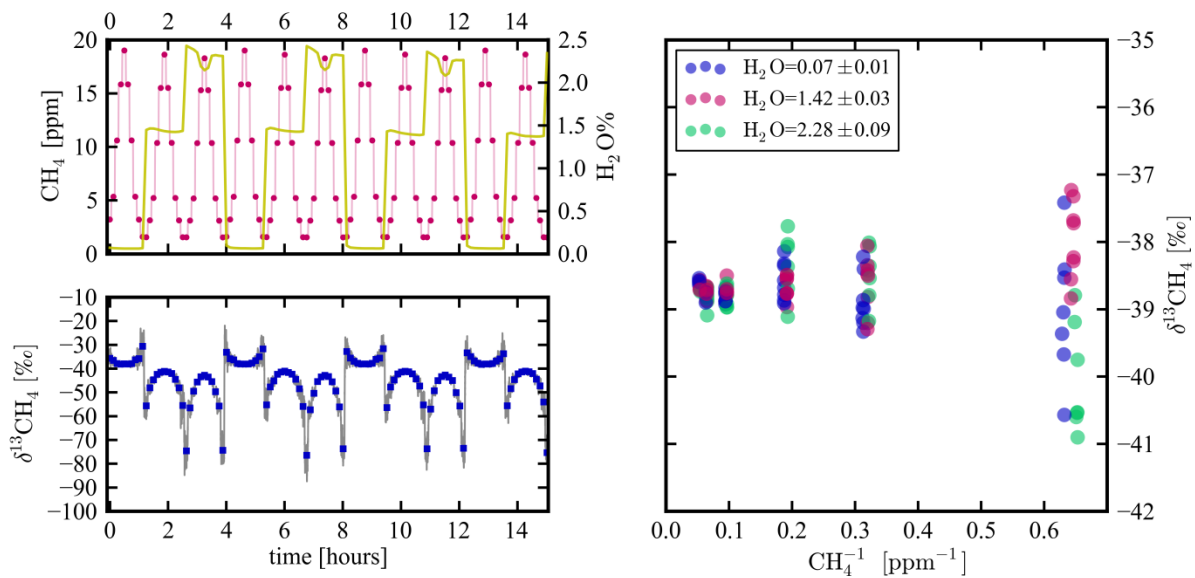


Figure S5: Time series of $\delta^{13}\text{CH}_4$ (bottom left panel, gray line) under changing water vapor and methane concentrations (top left panel, red and gold graphs, respectively). The mixtures are generated using the setup in Fig. 3. The blue points are an average from each 7.5 minute step. Both direct absorption and broadening effects are visible in the lower left panel. $\delta^{13}\text{CH}_4$ after correction using first order coefficients for water vapor direct absorbance and broadening, as discussed in the text.

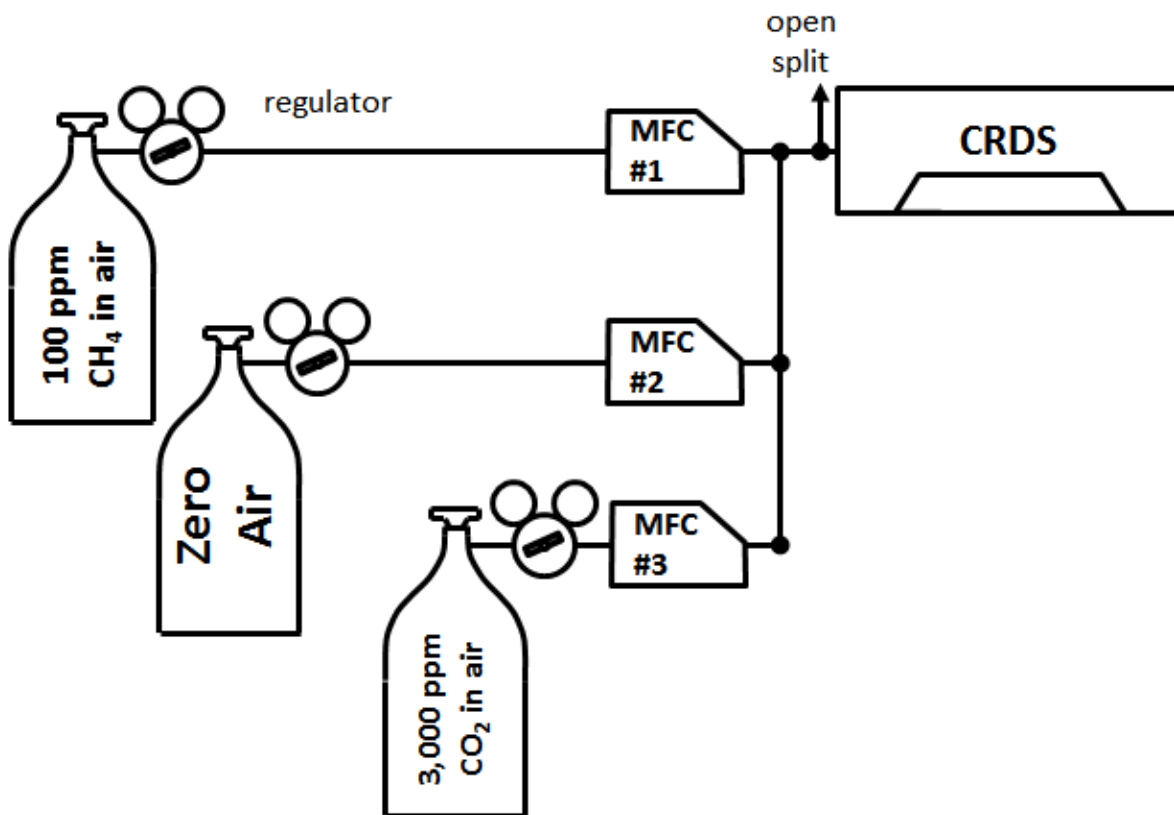


Figure S6: Setup for measuring the dependence of $\delta^{13}\text{CH}_4$ on carbon dioxide concentration. The flows are controlled using the MFCs to vary both CO₂ and CH₄ concentrations.

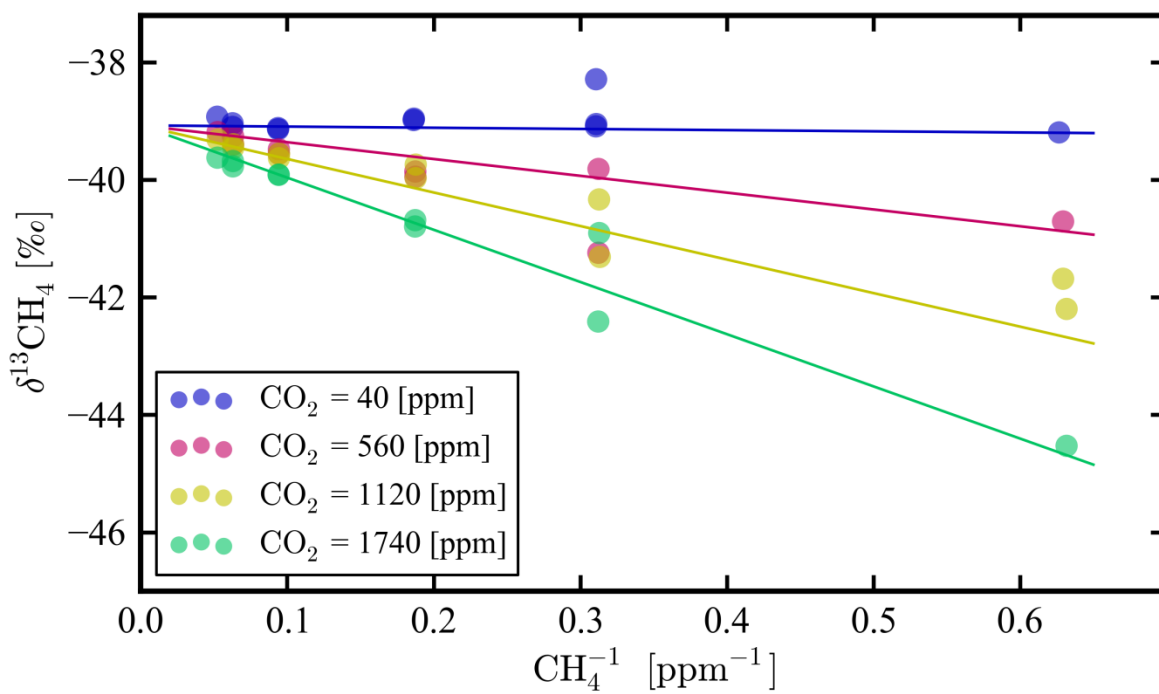


Figure S7: $(\delta^{13}\text{CH}_4)_{\text{raw}}$ signal as a function of methane concentration, for four different CO_2 concentrations, using the setup shown in Fig. 9. A small dependence on the CO_2 is visible. Also shown are the results of a least squares fit using the model function as described in the text.

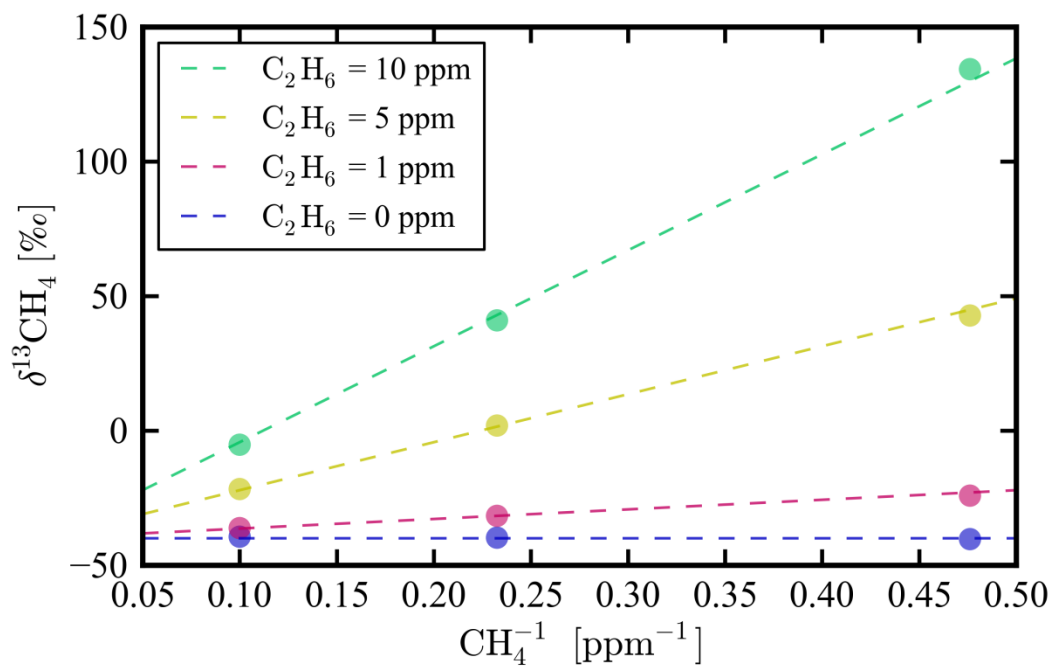


Figure S8: Dependence of $\delta^{13}\text{CH}_4$ on the measured ethane concentration, as a function of the reciprocal of the methane concentrations. A single correction coefficient of $35.6 \text{ ‰} - \text{ppm CH}_4 / \text{ppm C}_2\text{H}_6$ was used for the complete data set. The standard deviation of the fit residuals is 1.8 ‰ .

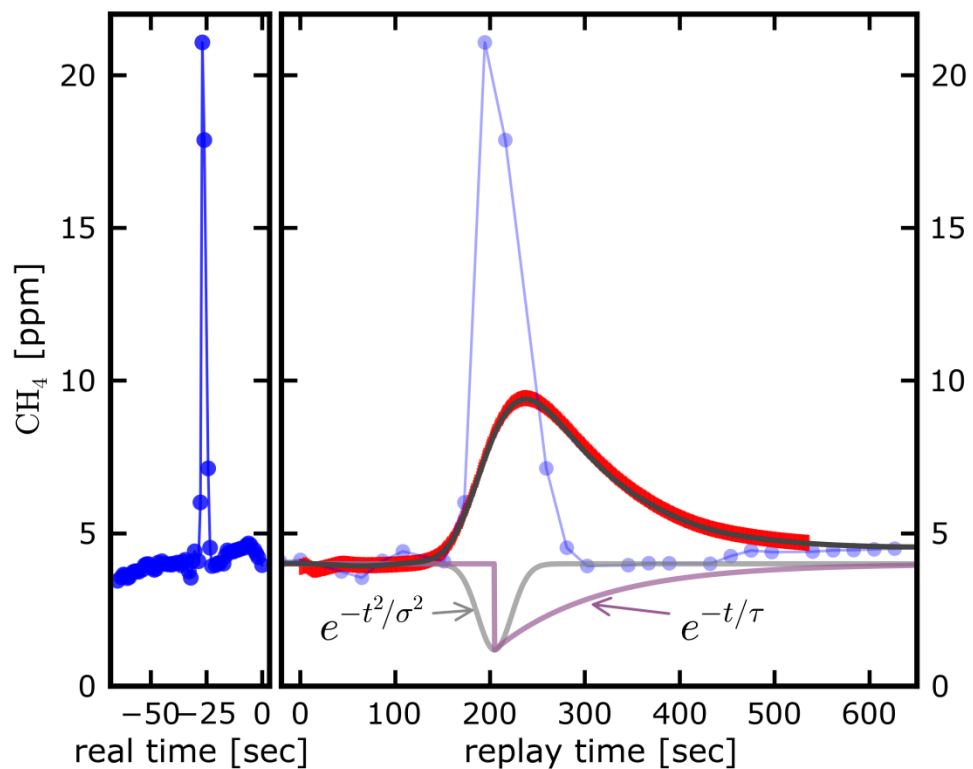


Figure S9: (left panel): measured transect through a typical natural gas plume. (right panel): measurement of the gas sample from the storage tube immediately after transecting the plume in the left panel (red). The direct plume measurement is reproduced in the right panel (blue), with the time axis scaled by a factor of 25. The Gaussian and exponential convolution functions are shown (gray and purple) on the same scaled time axis as the direct plume measurement. The convolution of the direct plume and the Gaussian and exponential is shown in black. The red data have been shifted in time to match up with the black curve, but no other adjustments have been made to the data.

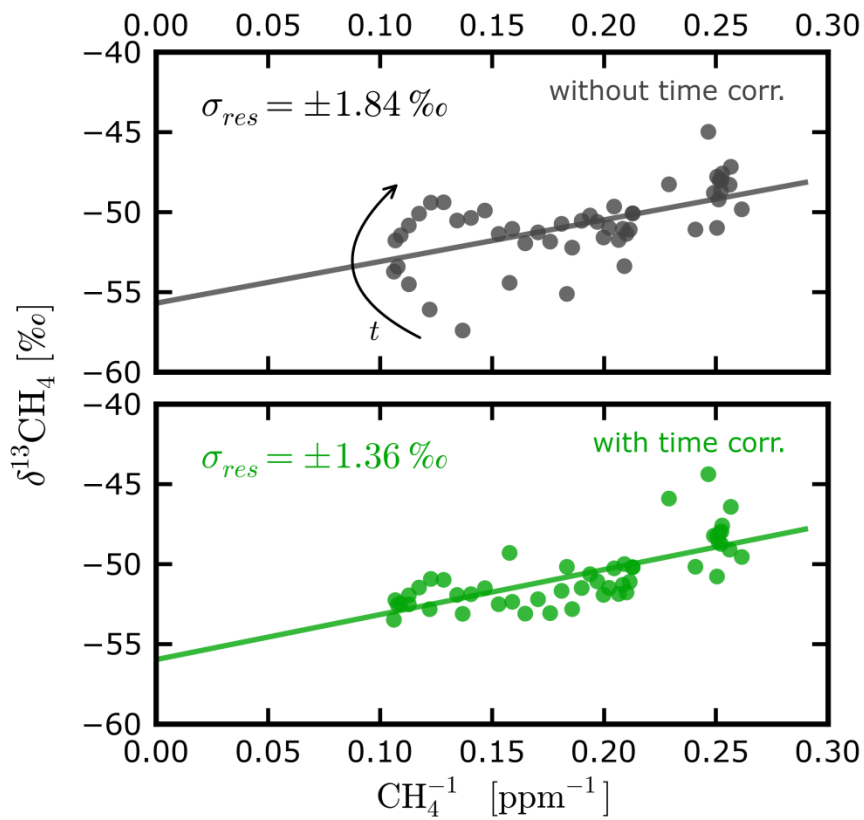


Figure S10: Top panel: Keeling plot of the plot shown in Fig 17, where the $^{13}\text{CH}_4$ data have not been time shifted. The data have been averaged over 6 data points, to reduce the noise. At high concentrations, there is a large variability, caused by the relative shift of $^{13}\text{CH}_4$ relative to $^{12}\text{CH}_4$. The direction of increasing time is indicated by the arrow on the figure. The y-intercept of the linear regression is $-55.7 \pm 1.4 \text{ ‰}$. Bottom panel: The same data, with a time lag of 0.5 seconds applied to the $^{13}\text{CH}_4$ data. The y-intercept of the linear regression is $-56.0 \pm 1.4 \text{ ‰}$. Note that for both data sets, $\delta^{13}\text{CH}_4$ has been corrected for ethane.

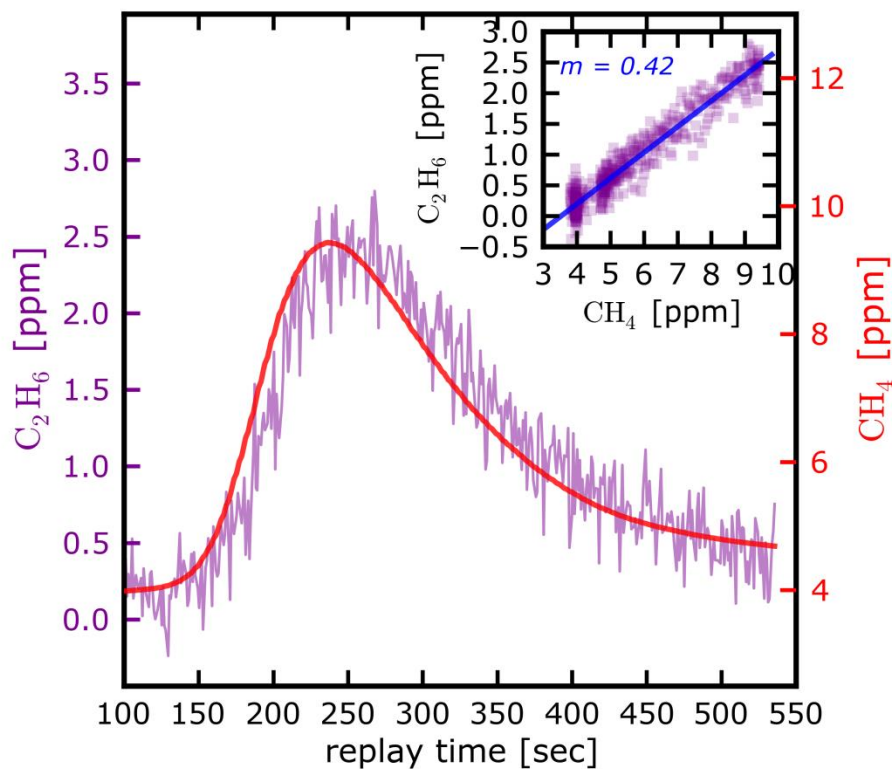


Figure S11: Measured ethane signal (purple, left axis) and methane (red, right axis). The ethane signal is delayed by about 10 seconds relative to the methane signal. The inset shows the correlation between the two species with the time shift applied, with a ratio of 42%.

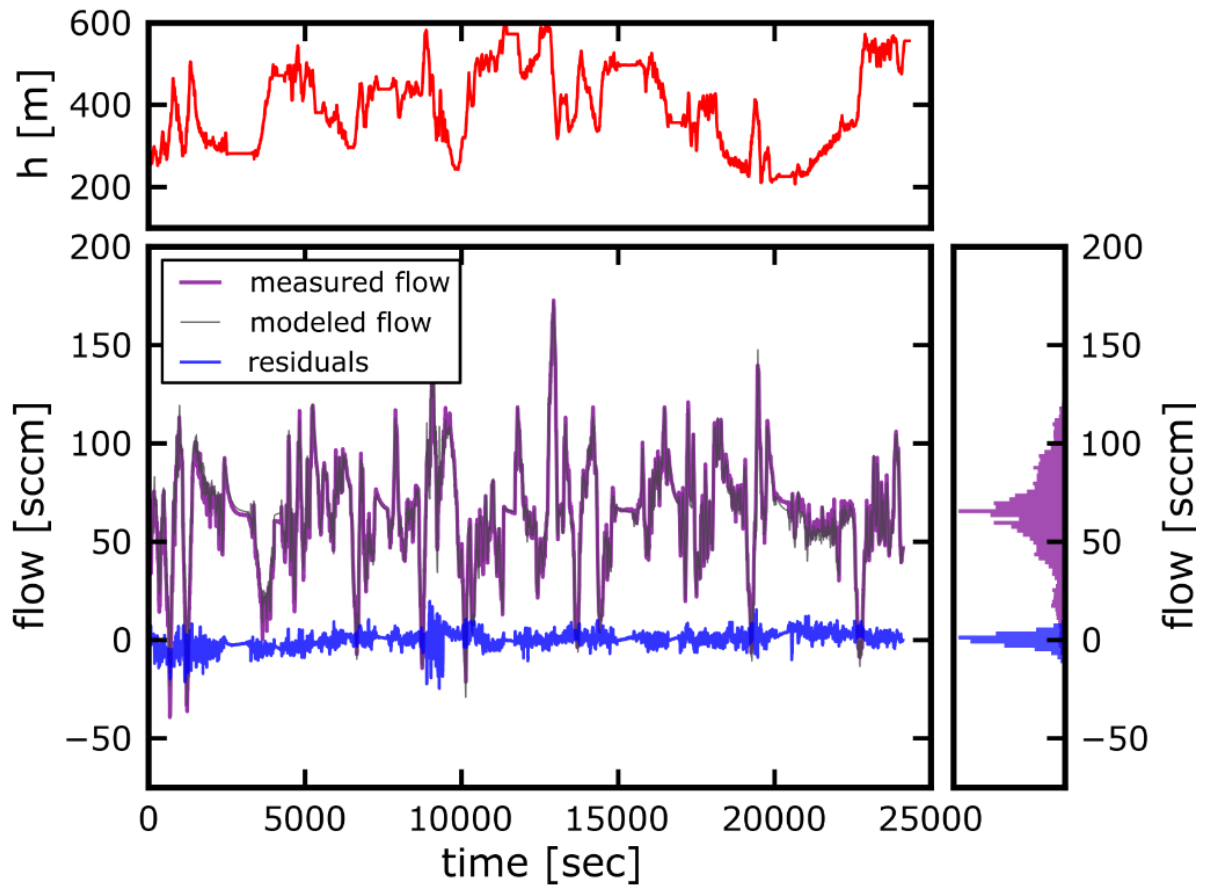


Fig S12. Central panel: Flow into the storage container (purple); modeled flow, as described in the text (gray); residuals (blue). Top Panel: Altitude profile for this drive. Right Panel: Histogram of measured flow (purple) and residuals (blue). The mean and standard deviation of the measured flow is 63 ± 26 sccm, and the standard deviation of the residuals is 3.8 sccm.

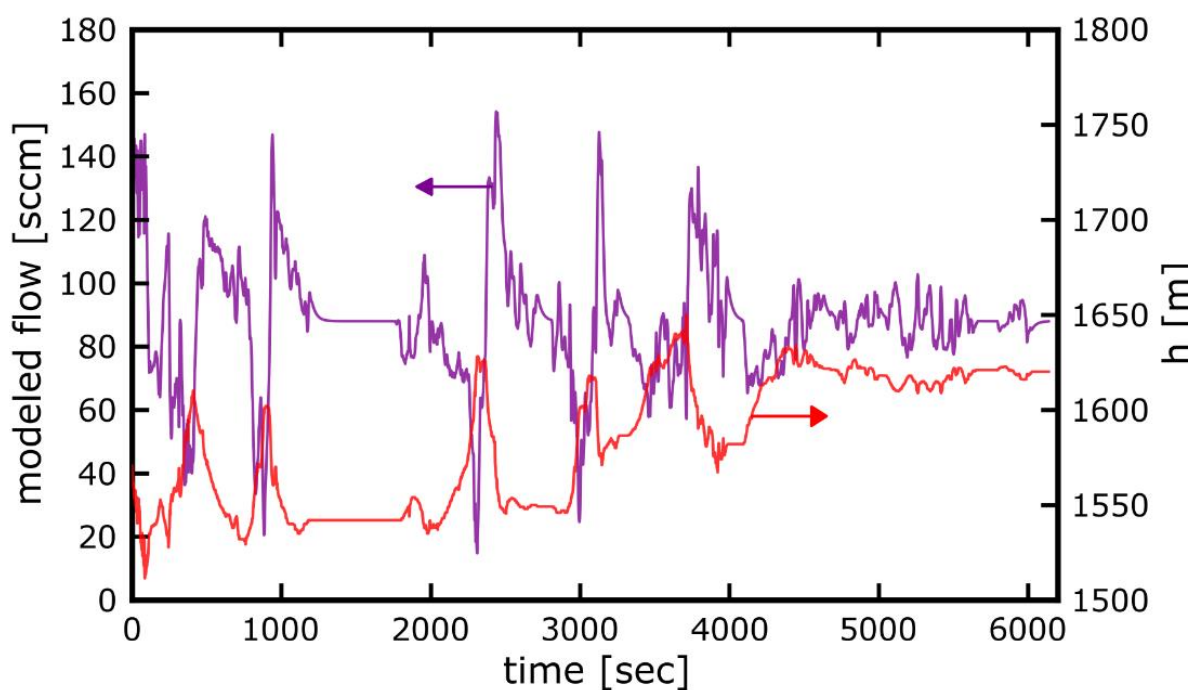


Figure S13. Vehicle altitude during measurement on 2014 0201 (red, right axis), along with the modeled flow based upon the vehicle altitude and speed. 95% of the flow variability is due to altitude changes, with just 5% due to speed changes. The modeled flow over the time period of the measurement is 88 ± 20 sccm (1-sigma).

S6 Supplementary Materials: References

- Bennett, C. O., & Myers, J. E. (1962). *Momentum, heat, and mass transfer*. New York: McGraw-Hill.
- Chen, H., Winderlich, J., Gerbig, C., Hofer, A., Rella, C. W., Crosson, E. R., Van Pelt, A. D., Steinbach, J., Kolle, O., Beck, V., Daube, B. C., Gottlieb, E. W., Chow, V. Y., Santoni, G. W., and Wofsy, S. C. (2010): High-accuracy continuous airborne measurements of greenhouse gases (CO₂ and CH₄) using the cavity ring-down spectroscopy (CRDS) technique, *Atmos. Meas. Tech.*, 3, 375-386.
- Johnson, T. J., Sams, R. L., & Sharpe, S. W. (2004, March). The PNNL quantitative infrared database for gas-phase sensing: a spectral library for environmental, hazmat, and public safety standoff detection. In *Optical Technologies for Industrial, Environmental, and Biological Sensing* (pp. 159-167). International Society for Optics and Photonics.
- Nara, H., Tanimoto, H., Tohjima, Y., Mukai, H., Nojiri, Y., Katsumata, K., & Rella, C. W. (2012). Effect of air composition (N₂, O₂, Ar, and H₂O) on CO₂ and CH₄ measurement by wavelength-scanned

cavity ring-down spectroscopy: calibration and measurement strategy. *Atmospheric Measurement Techniques*, 5(11), 2689-2701.

Marrero, T. R., & Mason, E. A. (1972). Gaseous diffusion coefficients. *Journal of Physical and Chemical Reference Data*, 1(1), 3-118.

Rella, C. W., Chen, H., Andrews, A. E., Filges, A., Gerbig, C., Hatakka, J., Karion, A., Miles, N. L., Richardson, S. J., Steinbacher, M., Sweeney, C., Wastine, B., and Zellweger, C.: High accuracy measurements of dry mole fractions of carbon dioxide and methane in humid air, *Atmos. Meas. Tech.*, 6, 837-860, doi:10.5194/amt-6-837-2013, 2013.

Rothman, L. S., Gordon, I. E., Babikov, Y., Barbe, A., Chris Benner, D., Bernath, P. F., ... & Wagner, G. (2013). The HITRAN2012 molecular spectroscopic database. *Journal of Quantitative Spectroscopy and Radiative Transfer*, 130, 4-50.

Varghese, P. L., & Hanson, R. K. (1984): Collisional narrowing effects on spectral line shapes measured at high resolution, *Applied Optics*, 23(14), 2376. OSA. doi:10.1364/AO.23.002376.